Brillouin characterization of slimmed polymer optical fibers for strain sensing with extremely wide dynamic range

YOSUKE MIZUNO,[1,*] NATSUKI MATSUTANI,[1] NEISEI HAYASHI,[2] HEEYOUNG LEE,[1] MASAKI TAHARA,[1] HIDEKI HOSODA,[1] AND KENTARO NAKAMURA[1]

[1]*Institute of Innovative Research, Tokyo Institute of Technology, 4259, Nagatsuta-cho, Midori-ku, Yokohama 226-8503, Japan*
[2]*Research Center for Advanced Science and Technology, The University of Tokyo, 4-6-1, Komaba, Meguro-ku, Tokyo 153-8904, Japan*
*ymizuno@sonic.pi.titech.ac.jp

Abstract: To date, most distributed Brillouin sensors for structural health monitoring have employed glass optical fibers as sensing fibers, but they are inherently fragile and cannot withstand strains of >3%. This means that the maximal detectable strain of glass-fiber-based Brillouin sensors was ~3%, which is far from being sufficient for monitoring the possible distortion caused by big earthquakes. To extend this strain dynamic range, polymer optical fibers (POFs) have been used as sensing fibers. As POFs can generally withstand even ~100% strain, at first, Brillouin scattering in POFs was expected to be useful in measuring such large strain. However, the maximal detectable strain using Brillouin scattering in POFs was found to be merely ~5%, because of a Brillouin-frequency-shift hopping phenomenon accompanied by a slimming effect peculiar to polymer materials. This conventional record of the strain dynamic range (5%) was still far from being sufficient. Here, we have thought of an idea that the strain dynamic range can be further extended by employing a POF with its whole length slimmed in advance and by avoiding the Brillouin-frequency-shift hopping. The experimental results reveal that, by applying 3.0% strain to a slimmed POF beforehand, we can achieve a >25% strain dynamic range, which is >5 times the conventional value and will greatly extend the application fields of fiber-optic Brillouin sensing.

1. Introduction

To implement smart materials and structures, fiber-optic strain and temperature sensing based on Brillouin scattering [1] has been a major target of research owing to its distributed measurement capability [2–12]. Most of the distributed Brillouin sensors reported so far have employed glass optical fibers (GOFs) as fibers under test (FUTs), and their Brillouin scattering properties have been well documented. However, GOFs cannot withstand strains of larger than ~3%, and consequently, it has been difficult to measure such large strains using GOF-based Brillouin sensors. In order to tackle this problem, some research groups [13,14] have attempted to use polymer optical fibers (POFs) as the FUTs of Brillouin sensors. POFs are known to be highly flexible and can sometimes withstand large strains of dozens of percent without considerable additional loss [15]. POF-based large-strain sensing has been already demonstrated using non-Brillouin methods by some research groups [16,17], but here we focus on Brillouin-based large-strain sensing using POFs, which can potentially be exploited to achieve distributed measurements in future.

Let us briefly trace the history of the study on Brillouin scattering in POFs. In 2010, the first observation of Brillouin scattering in a perfluorinated graded-index (PFGI-) POF [18], which is the only POF in which light can propagate with relatively low loss at telecom wavelength, was reported [19]. The Brillouin frequency shift (BFS) was found to be approximately 2.8 GHz at 1550 nm [19]. Then, the strain and temperature dependencies of

the BFS in the POFs were measured to be –122 MHz/% and –4.1 MHz/K at 1550 nm, respectively [20]. The absolute values are 0.2 and 3.5 times larger than those of silica GOFs, which indicates that it is difficult to employ Brillouin scattering in POFs to achieve highly sensitive strain sensing (when strain is relatively small). The BFS dependencies on larger strain [21] and wider-range temperature [22] have also been reported, which showed unique non-linear behaviors. To date, POFs have been successfully used to implement distributed sensing systems in the time [13], frequency [14], and correlation domains [23–25].

Thus, at the early stage of research, Brillouin scattering in POFs was expected to be useful in measuring large strains. However, as the large-strain dependence of the BFS [21] was further studied, it was found that, by applying strain of larger than ~5%, a POF locally starts to become slim with a constant outer diameter [26]. With increasing strain up to >60%, the slimmed section spreads along the whole length of the POF. The slimmed section has a BFS of approximately 3.2 GHz at 1550 nm, and thus, this slimming effect is inevitably accompanied by so-called BFS hopping. As the BFS is kept constant (only the Stokes powers change at ~2.8 and ~3.2 GHz) during this irreversible effect, the BFS in POFs cannot be directly used to measure strain of approximately 5–60%. Against this background, we have thought of an idea that the 5% limitation of the measurable strain can be extended further by employing a POF with its whole length slimmed in advance. The strain dependence of the BFS in the slimmed POF has been already measured, and the BFS is reported to linearly depend on strain with a coefficient of approximately –65.6 MHz/% at 1550 nm [26]. However, this report was only for relatively small strain of <1%. The BFS dependence on strain of >1% in the slimmed POF has not been clarified yet.

In this work, to extend the strain dynamic range, we investigate the BFS dependence on large strain in the slimmed POF. The BFS is found to be non-monotonically dependent on strain, in the same manner as in a non-slimmed POF, but without the BFS hopping phenomenon. With increasing strain, the BFS first decreases with a coefficient of –76.5 MHz/% (0–1.2% strain) and then increases with a coefficient of + 16.6 MHz/% (up to 30%). The BFS at 1.2–3.0% strain is almost independent of strain and cannot be directly used for strain sensing. In contrast, by applying 3.0% strain to a slimmed POF in advance, as large as >25% strain can be measured simply by using the one-to-one correspondence of the BFS to the strain. This strain dynamic range is at least 5 times as wide as the conventional value using a non-slimmed POF.

2. Principles

Light propagating along an optical fiber is in part returned via Brillouin scattering [1], and the spectrum of the back-propagated Stokes light is referred to as a Brillouin gain spectrum (BGS). The central frequency of the BGS is slightly lower than the pump frequency by the amount called a BFS. The BFSs of a silica single-mode fiber (SMF) and a PFGI-POF at 1550 nm are reported to be ~10.8 GHz [1] and ~2.8 GHz [19], respectively. If relatively small strain is applied to the SMF and the POF, their BFSs change with coefficients of 580 MHz/% [27] and –122 MHz/% [20], respectively. In the same manner, if the SMF and the POF are heated around room temperature, their BFSs change with coefficients of 1.2 MHz/K [28] and –3.2 MHz/K (or –4.1 MHz/K, depending on the fiber structure) [20,22], respectively.

An interesting phenomenon concerning Brillouin scattering in the largely strained POF is a BFS hopping phenomenon via a slimming effect [26]. When strain of larger than ~5% is applied to the POF, it partially starts to be slimmed in a stepwise manner (the slope of a stress-strain curve becomes almost zero at the elastic-to-plastic transition; refer to Appendix), maintaining a constant outer diameter (reduced by ~16% from a non-strained state). When the applied strain further increases, the slimmed section gradually spreads along the whole length of the POF. This slimming effect is reported to cause almost no additional optical loss [15]. This effect increases the density of the core of the POF, increasing the acoustic velocity, resulting in the BFS hopping from ~2.8 GHz to ~3.2 GHz at 1550 nm (corresponding to the

acoustic velocities of ~1600 and 1840 m/s, respectively; the BFS value after the slimming effect is highly repeatable). After this irreversible process, the coefficients of the BFS dependencies on strain (reported only for relatively small strain of <1%) and temperature (at around room temperature) have been reported to be –65.6 MHz/% and –4.04 MHz/K, respectively.

3. Methods

In the experiment for investigating the BFS dependence on larger strain in a slimmed POF, we employed a 0.58-m-long multimode PFGI-POF [18] as the FUT. The length of the POF was limited owing to the size of an experimental apparatus (guide rail) for applying strain. This POF had a three-layered structure consisting of core, cladding, and overcladding (diameters: 50, 70, and 490 μm; refractive indices: ~1.35, ~1.34, and 1.59, respectively). The materials of the core/cladding layers and the overcladding layer were doped/undoped amorphous perfluorinated polymers and polycarbonate, respectively. The numerical aperture was 0.185, and the propagation loss at 1550 nm was ~0.25 dB/m.

Figure 1 depicts an experimental setup, which is based on self-heterodyne detection and basically the same as that reported in our previous literature [19]. All the optical paths except the FUT were silica SMFs. The output from a laser diode (LD) at 1552 nm (linewidth: ~1 MHz) was divided into two beams: pump and reference. The pump light was amplified to 24 dBm using an erbium-doped fiber amplifier (EDFA) and injected into the POF (higher-power injection could increase the Brillouin signal, but we suppressed the power to avoid a so-called POF fuse effect with a relatively low threshold power) [29,30]. The Stokes light was amplified to 1 dBm using another EDFA. The reference light was also amplified to 1 dBm and coupled with the Stokes light for heterodyne detection. A polarization scrambler was inserted in the pump path to suppress the polarization-dependent signal fluctuations and to improve the measurement stability. The open end of the POF was attached to amorphous fluoropolymer to minimize the Fresnel reflection [31]. The optical beat signals were converted into electrical signals using a photodetector (PD) and observed using an electrical spectrum analyzer (ESA) as the BGS. The BGS was acquired after 100 times averaging on the ESA and fitted by a Lorentzian curve [1] to precisely deduce the BFS. The room temperature was 16 °C.
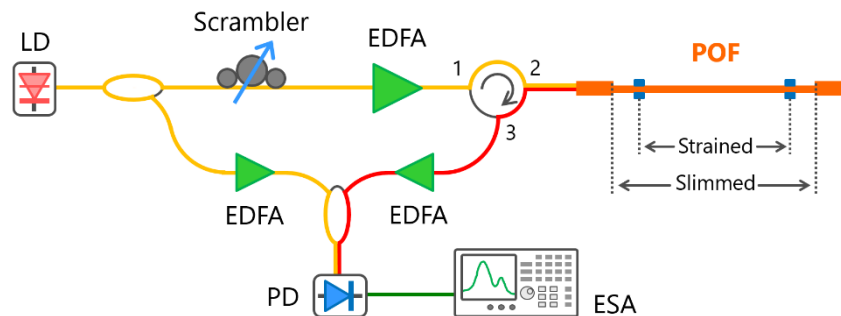

Fig. 1. Experimental setup for investigating the strain dependence of the BFS in a slimmed POF. EDFA: erbium-doped fiber amplifier, ESA: electrical spectrum analyzer, LD: laser diode, PD: photodetector.

The POF was fixed on translation stages using clamps. First, in order to create a slimmed section, strain of up to 80% was applied to the 0.36-m-long section around the middle of the POF at the strain rate of 2 mm/s. The applied strain of 80% was kept for 5 min, and then released, leading to the slimmed section with a length of 0.62 m. The BGS and BFS dependencies on strain were measured by applying strain to the 0.53-m-long section around the center of the slimmed section. The BGS and BFS showed transient response to the applied strain, but in this measurement, the convergent values (5 min after each strain was applied)

were used. The Stokes light backscattered from the POF included the Brillouin signals from the non-strained non-slimmed, non-strained slimmed, and strained slimmed sections. The third component is our target signal. The first component was automatically filtered out because its BFS is ~2.8 GHz. The second component cannot be easily filtered out, but its influence on the third is not significant, considering that its length (0.09 m) is much shorter than that of the third (0.53 m).

4. Results and discussions

Figure 2 shows the example of the BGS measured at 0.4% strain. In spite of the 100 times averaging, the spectral power was largely fluctuated because the height of the BGS was extremely low (much less than 1 dB). This is partly because the POF length was much shorter than those of previous reports [19,20] and partly because the clamped parts for applying large strain induced non-negligible optical loss. However, the BGS shape was well fitted by a Lorentzian curve, which resulted in the BFS of ~3.15 GHz. The standard deviation of the BFS fluctuations at relatively small strain (< 1%) was approximately 0.02% (evaluated using 10 pieces of data measured with an interval of 1 min).
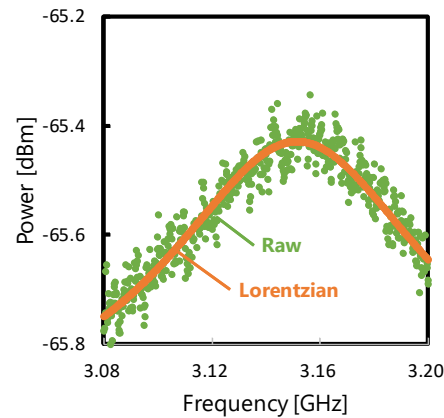

Fig. 2. BGS measured at 0.4% strain; raw data and its Lorentzian fit.

Figures 3(a) and 3(b) show the Lorentzian-fitted BGSs measured at strains of 0–2.0% and 5–30%, respectively. As the raw data contained non-essential noise-floor fluctuations, the vertical axis was normalized so that the maximal powers of each BGS became 0 dB. In Fig. 3(a), when the strain was small, the BGS shifted to lower frequency with increasing strain, but this trend ceased when the strain became larger. In Fig. 3(b), with increasing strain, the BGS shifted to higher frequency. The height of the BGS became gradually low probably because of the strain-induced acoustic loss (note that, as mentioned in Introduction, optical propagation loss is not significantly increased by large strain) [15]; when >35% strain was applied, the BGS was almost completely buried by the noise floor. The fluctuations of the Brillouin bandwidth are not essential and seem to have been caused by the noise-floor fluctuations and the modal instability. Note that the re-slimming effect of the once slimmed POF was not observed during this experiment (refer to Appendix).
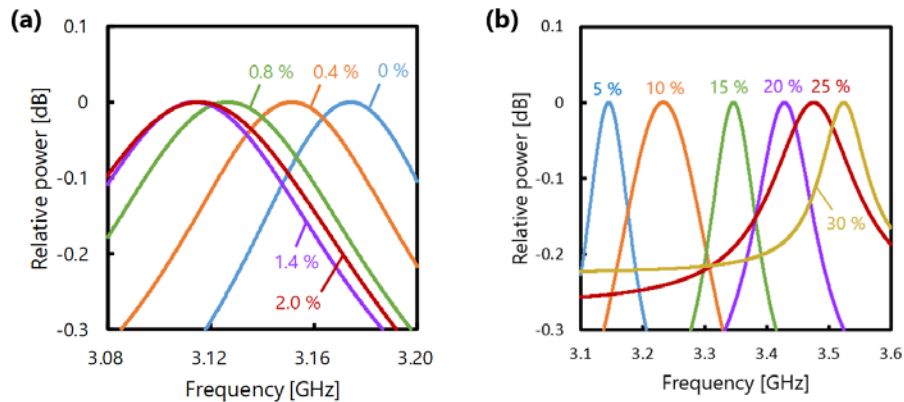
Fig. 3. Strain dependencies of the normalized Lorentzian-fitted BGSs measured in the strain ranges of (a) 0–2% and (b) 5–30%.

In order to quantitatively evaluate this behavior, the BFS was plotted as a function of the applied strain from 0 to 30% (Fig. 4). With increasing strain, the BFS first decreased (at strain smaller than ~1.2%) and then increased (up to 30%). This trend can be reasonably explained by its stress-strain curve (refer to Appendix) in the same manner as the trend in a non-slimmed POF (where the sign of the strain coefficient turns from negative to positive at ~2.5% (smaller than the strain at which the slimming effect starts)) [21]. We decided to investigate this trend by dividing the data into three strain ranges: 0–1.25%, 1.25–3.0%, and 3.0–30.0%.
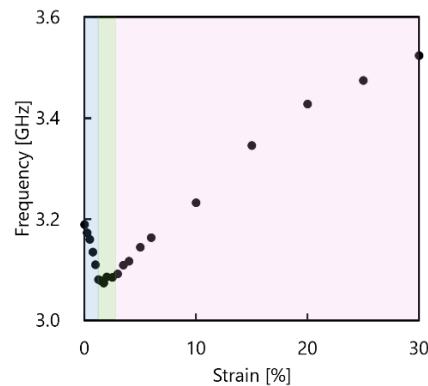

Fig. 4. BFS dependence on strain in the slimed POF. The colored regions indicate the three strain ranges magnified in Figs. 5(a)–(c).

Figure 5(a) shows the BFS dependence on strain at 0–1.25%. In this range, the BFS was almost linearly dependent on strain with a coefficient of –76.5 MHz/%. Its absolute value, which is ~7.6 times as small as that in a typical silica SMF [27], is larger than the previous report (65.6 MHz/% at <1.0%) measured at 20 °C. This could be valid considering the difference of the POF manufacturers (Asahi Glass in [26] and Sekisui Chemical in this paper) and the strain-temperature cross effect (specifically, the absolute value of the strain sensitivity is reported to become smaller with increasing temperature with a coefficient of 1.5 MHz/%/°C in a non-slimmed POF; see Fig. 3 of [26]). Subsequently, Fig. 5(b) shows the BFS dependence on strain at 1.25–3.0%. The BFS in this range was almost independent of strain, as the change in the BFS was comparable to the signal fluctuations caused by the low signal-to-noise ratio (see Fig. 2). Therefore, although the measurement precision is not high, this feature may potentially enable strain-insensitive temperature sensing by applying, for example, 2.0% strain to the slimmed POF beforehand. Finally, Fig. 5(c) shows the BFS

dependence on strain at 3.0–30.0%. In this range, with increasing strain, the BFS clearly increased. The strain coefficient became slightly smaller especially at >20.0% strain, but linear approximation roughly gave a coefficient of + 16.6 MHz/%. This value is approximately 1/35, 1/7.3, and 1/4.6 times the values (absolute values) in a typical silica SMF [27], a non-slimmed POF (at small strain) [20], and the slimmed POF (at <1.25% strain), respectively. Thus, although the strain sensitivity is extremely low, this behavior of the slimmed POF appears to be useful for rough measurement of large strain (note that the standard deviations of the BFS fluctuations in this strain range were > 0.1%). By applying 3.0% strain in advance, the one-to-one correspondence of the BFS to strain will be beneficial for simple implementation of such large-strain sensors (which can measure at least ~26% strain (= ~27 / 103)). Then, the achievable strain dynamic range will be >5 times wider than the conventionally widest value (~5%).
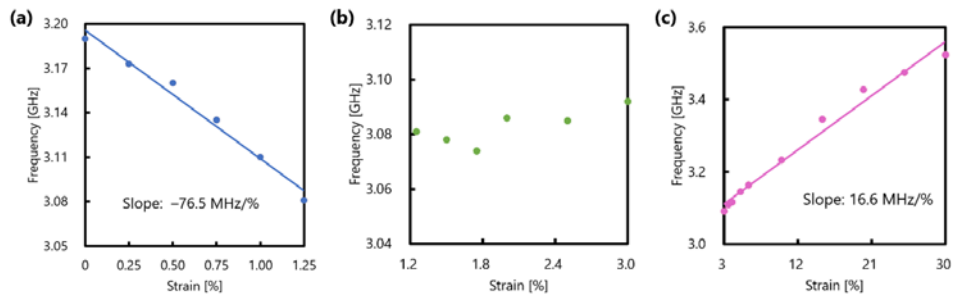

Fig. 5. Magnified views of the BFS dependence on strain in the slimed POF in the strain ranges of (a) 0–1.25%, (b) 1.25–3.0%, and (c) 3.0–30.0%. The solid lines in (a) and (c) are linear fits.

5. Conclusion

The BFS dependence on large strain in a slimmed POF was investigated to extend a strain dynamic range, which was conventionally limited to ~5%. We found that a BFS hopping phenomenon is not induced in the slimmed POF, and that with increasing strain, the BFS first decreases with a coefficient of –76.5 MHz/% (0–1.2% strain) and then increases with a coefficient of + 16.6 MHz/% (up to 30%). The BFS at 1.2–3.0% strain was almost independent of strain, which indicates strain sensing cannot be directly performed in this strain region unless the slimmed POF is pre-strained. We also showed that, by applying 3.0% strain to the slimmed POF beforehand, up to ~25% strain can be measured simply based on the one-to-one correspondence of the BFS to the strain. This strain dynamic range is at least 5 times as wide as the conventional value using a non-slimmed POF. We anticipate that this finding is of crucial importance in developing wide-dynamic-range strain sensing systems based on Brillouin scattering in POFs in the future. As a final remark, based on the experimental results, the research motivation of POF-based Brillouin sensing can be summarized as follows: when strain is relatively small and silica fibers can be directly (by their own deformation) used to measure the strain, high-sensitivity temperature sensing becomes feasible; in contrast, when strain is so large that silica fibers cannot be directly used, strain sensing is still feasible (even though the sensitivity is low).

Appendix: stress-strain curve of POF

The stress-strain curves of an 8.80-mm-long non-slimmed PFGI-POF in the strain ranges of 0–85% and 83–140% are shown in Figs. 6(a) and 6(b), respectively. These two figures were obtained continuously. The physical parameters of the PFGI-POF sample, including the core diameter (50 μm), were the same as those mentioned in Methods. The stress-strain curve was measured using a material testing machine (AG-5KN, Shimadzu). The strain rate was 25 μm/s, which is much slower than that of our previous report [21], leading to a more accurate

result. In Fig. 6(a), although the basic tendency was similar to the previous report, two dips were observed at ~9.5% and ~83%, which corresponded to the starting and ending points of the slimming process, respectively. During the slimming process, the stress was almost constant. In Fig. 6(b), with increasing strain, the stress basically increased and abruptly dropped to zero at ~137%. This drop was due to the breakage of the POF (at one of the clamped parts); when we set the strain of the slimmed POF (of which the whole length has just been slimmed) to 0%, the breakage strain can be calculated to be approximately 30% (= (237–183) / 183), which is close to the upper value of the strain range used in the BFS measurement (Fig. 4). We confirmed that the distortions of the stress-strain curve from the straight line in Fig. 6(b) (i.e., the dips at 93% and 120%, etc) were caused by the slipping of the POF at the clamped parts, indicating that, once a POF is slimmed, it does not experience a slimming effect again. This is because the slimming effect of this POF is caused by the yielding of the overcladding layer composed of polycarbonate. The core/cladding layers may exhibit the same effect, but along with the difference in material, their core diameters were so small compared to that of the overcladding that the re-slimming effect was not experimentally observed.
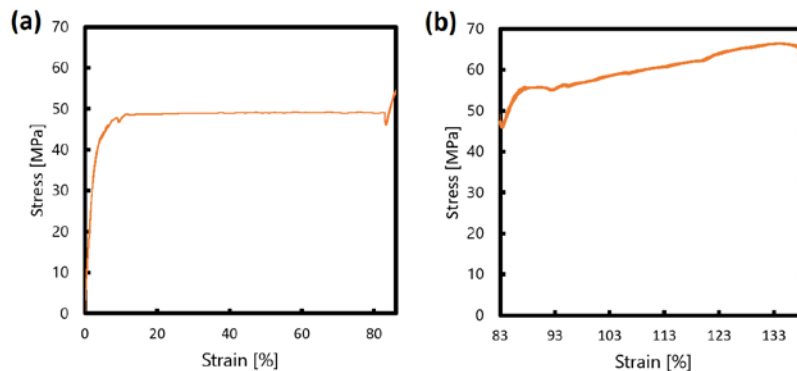

Fig. 6. Measured stress-strain curves of the POF in the strain ranges of (a) 0–85% and (b) 83–140%.

Funding

References

1. G. P. Agrawal, *Nonlinear Fiber Optics* (Academic, 2001).
2. M. Niklès and F. Ravet, "Distributed fibre sensors: Depth and sensitivity," Nat. Photonics **4**(7), 431–432 (2010).
3. T. Horiguchi and M. Tateda, "BOTDA–nondestructive measurement of single-mode optical fiber attenuation characteristics using Brillouin interaction: theory," J. Lightwave Technol. **7**(8), 1170–1176 (1989).
4. T. Kurashima, T. Horiguchi, H. Izumita, S. Furukawa, and Y. Koyamada, "Brillouin optical-fiber time domain reflectometry," IEICE Trans. Commun. **E76-B**(4), 382–390 (1993).
5. A. Denisov, M. A. Soto, and L. Thévenaz, "Going beyond 1000000 resolved points in a Brillouin distributed fiber sensor: theoretical analysis and experimental demonstration," Light Sci. Appl. **5**(5), e16074 (2016).
6. D. Zhou, Y. Dong, B. Wang, C. Pang, D. Ba, H. Zhang, Z. Lu, H. Li, and X. Bao, "Single-shot BOTDA based on an optical chirp chain probe wave for distributed ultra-fast measurement," Light Sci. Appl. **7**(1), 32 (2018).
7. D. Garus, K. Krebber, F. Schliep, and T. Gogolla, "Distributed sensing technique based on Brillouin optical-fiber frequency-domain analysis," Opt. Lett. **21**(17), 1402–1404 (1996).
8. Y. Antman, A. Clain, Y. London, and A. Zadok, "Optomechanical sensing of liquids outside standard fibers using forward stimulated Brillouin scattering," Optica **3**(5), 510–516 (2016).

9. K. Hotate and T. Hasegawa, "Measurement of Brillouin gain spectrum distribution along an optical fiber using a correlation-based technique–Proposal, experiment and simulation–," IEICE Trans. Electron. **E83-C**(3), 405–412 (2000).
10. Y. H. Kim, K. Lee, and K. Y. Song, "Brillouin optical correlation domain analysis with more than 1 million effective sensing points based on differential measurement," Opt. Express **23**(26), 33241–33248 (2015).
11. Y. Mizuno, W. Zou, Z. He, and K. Hotate, "Proposal of Brillouin optical correlation-domain reflectometry (BOCDR)," Opt. Express **16**(16), 12148–12153 (2008).
12. Y. Mizuno, N. Hayashi, H. Fukuda, K. Y. Song, and K. Nakamura, "Ultrahigh-speed distributed Brillouin reflectometry," Light Sci. Appl. **5**(12), e16184 (2016).
13. Y. Dong, P. Xu, H. Zhang, Z. Lu, L. Chen, and X. Bao, "Characterization of evolution of mode coupling in a graded-index polymer optical fiber by using Brillouin optical time-domain analysis," Opt. Express **22**(22), 26510–26516 (2014).
14. A. Minardo, R. Bernini, and L. Zeni, "Distributed temperature sensing in polymer optical fiber by BOFDA," IEEE Photonics Technol. Lett. **26**(4), 387–390 (2014).
15. H. Ujihara, N. Hayashi, Y. Mizuno, and K. Nakamura, "Measurement of large-strain dependence of optical propagation loss in perfluorinated polymer fibers for use in seismic diagnosis," IEICE Electron. Express **11**(17), 20140707 (2014).
16. T. Chen, J. Tu, X. Song, and Z. Li, "Sensor for measuring extremely large strain based on bending polymer optical fiber," Instrum. Exp. Tech. **60**(2), 301–306 (2017).
17. D. Q. Ying, X. M. Tao, W. Zheng, and G. F. Wang, "Fabric strain sensor integrated with looped polymeric optical fiber with large angled V-shaped notches," Smart Mater. Struct. **22**(1), 015004 (2012).
18. Y. Koike and M. Asai, "The future of plastic optical fiber," NPG Asia Mater. **1**(1), 22–28 (2009).
19. Y. Mizuno and K. Nakamura, "Experimental study of Brillouin scattering in perfluorinated polymer optical fiber at telecommunication wavelength," Appl. Phys. Lett. **97**(2), 021103 (2010).
20. Y. Mizuno and K. Nakamura, "Potential of Brillouin scattering in polymer optical fiber for strain-insensitive high-accuracy temperature sensing," Opt. Lett. **35**(23), 3985–3987 (2010).
21. N. Hayashi, Y. Mizuno, and K. Nakamura, "Brillouin gain spectrum dependence on large strain in perfluorinated graded-index polymer optical fiber," Opt. Express **20**(19), 21101–21106 (2012).
22. K. Minakawa, N. Hayashi, Y. Shinohara, M. Tahara, H. Hosoda, Y. Mizuno, and K. Nakamura, "Wide-range temperature dependences of Brillouin scattering properties in polymer optical fiber," Jpn. J. Appl. Phys. **53**(4), 042502 (2014).
23. N. Hayashi, Y. Mizuno, and K. Nakamura, "Distributed Brillouin sensing with centimeter-order spatial resolution in polymer optical fibers," J. Lightwave Technol. **32**(21), 3999–4003 (2014).
24. H. Lee, N. Hayashi, Y. Mizuno, and K. Nakamura, "Slope-assisted Brillouin optical correlation-domain reflectometry using polymer optical fibers with high propagation loss," J. Lightwave Technol. **35**(11), 2306–2310 (2017).
25. N. Hayashi, Y. Mizuno, and K. Nakamura, "Simplified Brillouin optical correlation-domain reflectometry using polymer optical fiber," IEEE Photonics J. **7**(1), 6800407 (2015).
26. N. Hayashi, K. Minakawa, Y. Mizuno, and K. Nakamura, "Brillouin frequency shift hopping in polymer optical fiber," Appl. Phys. Lett. **105**(9), 091113 (2014).
27. T. Horiguchi, T. Kurashima, and M. Tateda, "Tensile strain dependence of Brillouin frequency shift in silica optical fibers," IEEE Photonics Technol. Lett. **1**(5), 107–108 (1989).
28. T. Kurashima, M. Tateda, and M. Tateda, "Thermal effects on the Brillouin frequency shift in jacketed optical silica fibers," Appl. Opt. **29**(15), 2219–2222 (1990).
29. Y. Mizuno, N. Hayashi, H. Tanaka, K. Nakamura, and S. Todoroki, "Observation of polymer optical fiber fuse," Appl. Phys. Lett. **104**(4), 043302 (2014).
30. Y. Mizuno, N. Hayashi, H. Tanaka, K. Nakamura, and S. Todoroki, "Propagation mechanism of polymer optical fiber fuse," Sci. Rep. **4**(1), 4800 (2014).
31. N. Matsutani, H. Lee, Y. Mizuno, and K. Nakamura, "Long-term stability enhancement of Brillouin measurement in polymer optical fibers using amorphous fluoropolymer," Jpn. J. Appl. Phys. **57**(1), 018001 (2018).